Dynamics of electronically excited states in the eumelanin building block 5,6-dihydroxyindole

Dynamics of electronically excited states in the eumelanin building block 5,6-dihydroxyindole†

Stuart W. Crane[1,‡], Omair Ghafur[1], Thomas Y. Cowie[2], Anita G. Lindsay[2], James O. F. Thompson[1,§], Jason B. Greenwood[3], Magnus W. P. Bebbington[2,4] and Dave Townsend[1,2,*]

[1] *Institute of Photonics & Quantum Sciences, Heriot-Watt University, Edinburgh, EH14 4AS, UK*

[2] *Institute of Chemical Sciences, Heriot-Watt University, Edinburgh, EH14 4AS, UK*

[3] *School of Mathematics and Physics, Queen's University Belfast, Belfast BT7 1NN, UK*

[4] *Department of Chemistry & Biochemistry, Montclair State University, Montclair, NJ 07043, USA*

Abstract

We report the first excited state dynamics study of gas-phase 5,6-dihydroxyindole (5,6-DHI), a key building block of eumelanin pigments that are found throughout nature and serve as important photo-protective compounds. Time-resolved ion-yield measurements over the 241-296 nm ultraviolet photoexcitation region revealed non-adiabatic processes occurring on up to three distinct timescales. These reflect ultrafast (i.e. sub-picosecond) internal conversion within the excited state singlet manifold, and much longer-lived processes ranging from 10 ps to in excess of 1 ns. Our investigation paves the way for precisely targeted future studies of 5,6-DHI that exploit more differential measurement techniques. The work was facilitated by the use of soft laser-based thermal desorption to introduce 5,6-DHI samples into the gas phase. This approach, based on low-cost, readily available diode lasers, is straightforward, easily controllable and potentially applicable to a wide range of non-volatile molecular species.

† Electronic supplementary information (ESI) available: Synthetic procedures and sample characterization.

‡ Present address: School of Chemistry, University of Bristol, Cantock's Close, Bristol, BS8 1TS, United Kingdom

§ Present address: School of Chemistry, University of Nottingham, Nottingham, NG7 2RD, United Kingdom

* Corresponding author: e-mail d.townsend@hw.ac.uk,

I. INTRODUCTION

Skin, the largest organ of the human body, serves as a first point of contact with the external environment. Various biological and physical characteristics of the skin dictate its ability to resist repeated exposure to damaging environmental stimuli, with one particularly important example being the production of photo-protective melanin pigments upon exposure to ultraviolet (UV) light. The most common form of melanin in humans is eumelanin, which colours the skin, hair, and retina, and exhibits a broad absorption across the UV region. Despite its obvious importance, numerous spectroscopic studies conducted over the past two decades have yet to reveal a complete picture of the eumelanin photo-protective mechanism.[1-6] This is, in part, due to melanin pigments having a complex and ill-defined amorphous structure. Furthermore, theoretical investigations in this area have been quite limited in number – especially those regarding electronically excited states. A recent publication by Marchetti *et al.*[7] has, however, provided a theoretical insight into the UV relaxation dynamics operating in a selection of dimer and trimer combinations made from the principal monomeric building block units of eumelanin; 5,6-dihydroxyindole (5,6-DHI) and 5,6-dihydroxyindole-2-carboxylic acid (5,6-DHICA). The structures of these species are presented in Fig. 1, along with the carbon/oxygen position-numbering scheme that will be referred to at numerous points throughout. This study revealed the presence of a barrierless ultrafast electron driven proton transfer pathway from the initially excited $S_1(\pi\pi^*)$ state to an S_1/S_0 crossing, although further investigations are required to more fully understand the relaxation schemes in operation.

Here we report the results of an ultrafast time-resolved ion-yield (TRIY) study investigating the non-adiabatic dynamics of 5,6-DHI following excitation across the 241-296 nm region.

Although 5,6-DHI and 5,6-DHICA have been studied extensively in solution,[8-15] our work is, to the best of our knowledge, the first gas phase excited state dynamics study to be conducted on either system. Gas phase measurements are an important "bottom-up" starting point that provide critical new benchmarks for advanced theory under conditions that are free from solvent perturbations. One drawback here is that the very low vapour pressure of 5,6-DHI makes gas-phase study challenging by conventional molecular beam methods, and our previous attempts to use this type approach gave signal levels that were far too low for reliable pump-probe measurements. This issue has been overcome, however, through the use of a laser-based thermal desorption approach that we have previously demonstrated for the uracil and 2-thiouracil systems.[16] This technique has the potential to facilitate vapour generation in a broad range of non-volatile species and we anticipate it will find wider application beyond the work outlined here.

The 5,6-DHI system has been the subject of several previous theoretical studies investigating its molecular structure and photophysical properties. Of particular relevance to our present work are a small selection of reports focusing on non-adiabatic excited state processes. In the first of these, *ab initio* investigations undertaken by Sobolewski and Domcke considered excitation to the optically bright $S_1(\pi\pi^*)$ state.[17] Extension along the O5-H stretching coordinate was shown to be a critical motion for facilitating internal conversion to the $S_2(\pi\sigma^*)$ state. Furthermore, hydrogen atom migration was then predicted from the O5 position to the neighboring C4 atom, forming the photoproduct 6-hydroxy-4-dihydro-indol-5-one (HHI). This species was predicted to absorb strongly in the visible region of the spectrum, transitioning to a $\pi\pi^*$ state prior to rapid relaxation to the HHI ground state.

A more recent study by Datar and Hazra, employing state-averaged complete active space self-consistent field (SA-CASSCF) methods, has provided an alternative description of the energy dissipation pathways.[18] These authors suggest the $S_2(\pi\sigma^*)$ state has a bound minimum energy geometry rather than a barrierless pathway for hydrogen migration. Potential energy scans along the O5-H and N-H stretching coordinates revealed two possible deactivation routes for the $S_2(\pi\sigma^*)$ state, once populated from $S_1(\pi\pi^*)$ via internal conversion. Both of these displayed a barrier to H atom dissociation, although this was found to be significantly lower along the O5-H pathway (0.30 eV, compared to 0.63 eV along the N-H coordinate). An additional deactivation pathway involving ring-puckering motions was also found directly between the $S_1(\pi\pi^*)$ state and the S_0 ground state, with a small barrier again being present. Relaxation from the second, higher lying optically bright $^1\pi\pi^*$ state was suggested to occur via a barrierless conical intersection to $S_1(\pi\pi^*)$. This study also concluded that the antibonding σ^* orbital associated with the O6-H coordinate was much higher in energy than the corresponding O5-H σ^* orbital. This was attributed to the interaction between the σ^* molecular orbital along the O6-H stretching coordinate and a nonbonding orbital on the oxygen atom at the C5 position that acts as a hydrogen bond acceptor.

Work by Ghosh and Ghosh also employed SA-CASSCF and multistate complete active space second-order perturbation theory (MS-CASPT2) calculations to investigate non-radiative decay pathways in 5,6-DHI.[19] Potential energy cuts comparable to those of Datar and Hazra were evaluated along the O5-H and N-H stretching coordinates, and similar conclusions were reached regarding the fate of the $S_1(\pi\pi^*)$ state (i.e. non-radiative decay to $S_2(\pi\sigma^*)$ prior to encountering a further conical intersection with the S_0 ground state at highly extended bond lengths). A barrier was again seen to be present between the $S_2(\pi\sigma^*)$ state and S_0 along both the O5-H and N-H

stretching coordinates, with that along O5-H found to be energetically lower. Furthermore, these authors also investigated the morphology of the $S_2(\pi\sigma^*)/S_0$ conical intersections (CI) upon elongation of the O5-H and N-H bonds. The symmetric nature of the CI in the former case was predicted to lead to an equal propensity for non-radiative decay to the ground state *vs* excited state H-atom elimination/radical formation. In contrast, the CI accessed along the N-H stretching coordinate was found to be directed along the g-vector (gradient difference vector),[20] leading to a reduced probability of returning non-radiatively to S_0.

A further set of molecules one may use for instructive comparison with 5,6-DHI are the monohydroxyindoles, 4-, 5- and 6-hydroxyindole (4-HI, 5-HI and 6-HI), the structures of which are also included in Fig. 1. Of particular note here are the H-atom photofragment translation energy distributions from 4-HI and 5-HI reported by Ashfold and co-workers.[21] In the case of 4-HI, this work concluded high kinetic energy H atoms were formed predominantly from excited state O-H bond fission over a broad range of excitation wavelengths (303.9 – 193.3 nm). In contrast, 5-HI displayed markedly different behaviour, with N-H bond fission being the dominant contributor to high kinetic energy H atom production at excitation wavelengths >235 nm. This picture is supported by the time-resolved photoelectron spectroscopy studies of Livingstone *et al*. that made direct comparisons between the excited state dynamics operating in indole and 5-HI.[22] At pump wavelengths of 249 nm and 273 nm both molecules were observed to exhibit very similar behaviour, reinforcing the idea that motion along the N-H coordinate is a key factor is driving the electronic relaxation and the O-H bond in 5-HI acts as a spectator. The influence of substituent position on UV-induced dynamics is also suggested in helium jet fluorescence studies of the mono-hydroxyindoles following excitation close to their S_1 origins, with 4-HI displaying a far shorter lifetime (0.2 ns),[23] than either 5-HI or 6-HI (11.1 ns and 2.8 ns, respectively).[24, 25] We also highlight

here that further dynamical differences between 5,6-DHI and the monohydroxyindoles might also reasonably be expected by analogy with, for example, phenol (hydroxybenzene) and catechol (1,2-dihydroxybenzene). The $S_1(\pi\pi^*)$ excited state lifetime of catechol is 1-2 orders of magnitude shorter than in phenol – an observation attributed to differences in the rate of H atom tunnelling through the barrier formed by a conical intersection between the $S_1(\pi\pi^*)$ state and the $S_2(\pi\sigma^*)$ state (which is dissociative along the O–H stretching coordinate).[26-29]

II. EXPERIMENTAL

Samples of 5,6-DHI were prepared "in-house" in four synthetic steps from 3,4-dibenzyloxybenzaldehyde and via 5,6-dibenzyloxyindole. Detailed procedures are described elsewhere.[30, 31] Deuterated samples were produced by dissolving 5,6-DHI in D_2O, stirring at room temperature for 2 hours and then evaporating. This yielded >95% deuterium substitution at the O5-H, O6-H and N-H positions, as confirmed by mass spectrometry and NMR analysis. Further synthetic details are provided in the electronic supplementary information (ESI).

For preliminary comparative UV absorption spectra measurements, samples of 4-HI, 5-HI, 6-HI and indole (all 97% purity or above) were purchased from Sigma-Aldrich and used without further refinement. Absorption spectra were recorded for all molecules using a commercial bench-top UV/visible spectrophotometer (Shimadzu UV-2550) over the wavelength range 225–325 nm. Samples were dissolved in cyclohexane due to the non-volatile nature of some species, in particular 5,6-DHI, which has a predicted vapour pressure on the order of 10^{-5} – 10^{-6} mmHg at 25 °C.[32] Cyclohexane is a non-polar solvent and is therefore expected to provide a good proxy to the gas-phase environment. Furthermore, it has minimal UV absorption at wavelengths >195 nm and therefore does not exhibit any spectral features over the sampled UV range.

Time-resolved ion-yield experiments were conducted using a newly built ultra-high vacuum spectrometer dedicated to the gas-phase study of non-volatile species. This instrument incorporates a laser desorption source based on the design of Greenwood and co-workers,[33, 34] and has recently been described in detail elsewhere.[16] Briefly, the source consisted of a piece of 10 μm thick 316 stainless steel foil (Ø = 32 mm) onto which 5,6-DHI powder was deposited using application of methanol. This produced a uniform coating 300-500 μm thick. The foil was then clamped within the repeller electrode forming part of an ion optics assembly that accelerated charged species towards a detector following pump/probe laser ionization. The focused 445 nm output from a CW laser diode (Kale CNC) was used to irradiate the rear (i.e. uncoated) side of the foil to produce a plume of 5,6-DHI in the gas phase. The center of the circular foil was displaced from the central time-of-flight axis running along the instrument. Rotation of the foil within the repeller electrode (accomplished via an air-to-vacuum feedthrough and simple gear assembly) therefore allowed the sample to be periodically replenished. The thinness of the foil and the low thermal conductivity of stainless steel ensured 445 nm absorption generated a confined hotspot from which molecules underwent thermally induced desorption. The temperature and area of this spot was controlled by adjusting the voltage supplied to the diode and/or by varying the focusing conditions. These parameters were typically set to produce a laser power of ~150 mW and a spot on the foil ~1 mm in diameter, yielding a localized estimated foil temperature of ~370 ± 30 K, as detailed in earlier work using this instrument.[16] Calculations by Il'ichev and Simon have shown the 5,6-DHI tautomer depicted in Fig. 1 to be the lowest energy form both in the gas-phase and when solvated.[35] All other tautomers were found to lie > 1300 cm^{-1} higher in energy. Given the modest sample temperatures produced by the laser-based thermal desorption approach used in our present

investigation, only the lowest energy tautomer of 5,6-DHI was therefore expected in the sample plume generated above the foil surface.

The ultrafast laser employed for the TRIY experiments was a 3.8 W, 1 kHz, regeneratively amplified Ti:Sapphire system (Spectra-Physics, Spitfire Pro/Empower) seeded by a Ti:Sapphire oscillator (Spectra-Physics, Tsunami/Millennia). The 800 nm central wavelength output was divided using multiple beam-splitters, with one component of this being employed directly as an intense multiphoton probe (70 fs FWHM, 130 μJ/pulse, $\sim 2 \times 10^{13}$ W/cm^2 when focused). Recording some test data sets at reduced intensity confirmed that the probe does not actively perturb the observed dynamics. A second component of the 800 nm light was used as the input for an optical parametric amplifier (Spectra-Physics OPA-800C), the signal or idler output of which was then sum-frequency mixed with a third component of the 800 nm fundamental inside a thin β-barium borate (BBO) crystal. This produced light in the visible spectral region, which was then frequency doubled into the UV using a second thin BBO crystal. UV pump pulses were generated over the 241-296 nm region using this approach. One exception was 267 nm (the third harmonic of the 800 nm fundamental) which was produced via a simple 800 nm frequency-tripling scheme in two successive BBO crystals. Pump powers used in the experiments were dependent upon wavelength generation efficiency, and ranged between 0.2 – 1.0 μJ/pulse. The pump and probe and were collinearly combined using a thin dichroic mirror before entering the spectrometer via a 1 mm thick CaF_2 window. Focusing was achieved independently (i.e. pre-combination) via fused silica (f = 50 cm) and calcium fluoride (f = 63 cm) plano-convex lenses, respectively. The pump and probe beams had parallel polarizations directed perpendicular to the spectrometer time-of-flight axis.

The desorbed plume of 5,6-DHI molecules and the pump/probe laser pulses underwent interaction ~2-3 mm above the foil surface. The ions produced were then accelerated along a short flight tube towards a dual micro-channel plate/phosphor screen detector. The resulting light emitted was then detected by a fast silicon photomultiplier positioned external to the vacuum. At each pump-probe delay position, Δt, the output from the photomultiplier was recorded by an oscilloscope interfaced to a PC running custom MATLAB data acquisition code. This software also controlled an automated high-precision delay stage fitted with a retro-reflector (placed in the probe beamline) and a pair of homemade shutters that permitted pump-alone and probe-alone background signals to be recorded at each pump-probe position, as required. Data collection runs repeatedly sampled a series of small linear steps at short pump-probe delay times and larger, exponentially increasing increments out to 200 ps (the limit of the delay stage) to capture the more extended system dynamics. Prior to commencing data collection, 1,3-butadiene was introduced into the interaction region via a needle valve in order to perform cross-correlation measurements, provide time-of-flight calibration and also to accurately determine the experimental time-zero (i.e. $\Delta t = 0$) position.

The temporal evolution of our data was analyzed using a sequential Levenberg-Marquardt fitting routine wherein the transient ionization signals $S(\Delta t)$ were described as:

$$S(\Delta t) = \sum_{i=1}^{n} P_i(\Delta t) \otimes g(\Delta t) \qquad (1)$$

Here $g(\Delta t)$ denotes the experimentally determined Gaussian cross-correlation (which ranged between 160 - 110 fs over the 241- 296 nm pump region). A series of n exponentially decaying functions $P_i(\Delta t)$, each with an associated fit amplitude a_i, were defined as follows:

$$P_i(\Delta t) = a_i \exp[-\Delta t/\tau_i] \qquad (i=1)$$

$$P_i(\Delta t) = a_i \exp[-\Delta t/\tau_i]\left(1-\exp[-\Delta t/\tau_{i-1}]\right) \qquad (i>1) \tag{2}$$

The 5,6-DHI parent ion transients required either a one, two or three exponential fitting model, depending upon the specific excitation wavelength.

III. RESULTS

A. UV Absorption Spectra

The UV absorption spectra (in cyclohexane) recorded for 5,6-DHI, the mono-hydroxyindoles 4-HI, 5-HI and 6-HI, and the hydroxyl-free chromophore indole are presented in Fig. 2. The spectra of indole and 5-HI are very similar to those previously reported in the gas-phase by Livingstone *et al.*,[22] confirming that the cyclohexane solvent only weakly perturbs the absorption seen in the free molecules. When compared to indole, all hydroxylated species display red-shifted absorption features. In 4-HI the onset of the first two bands is only slightly lowered in energy, whereas this shift becomes significantly more pronounced in 6-HI. The biggest shifts, however, are seen in 5-HI and 5,6-DHI, both of which exhibit strikingly similar overall spectra. This is a particularly useful finding as it permits instructive comparisons between the dynamics observed in 5-HI and 5,6-DHI at equivalent excitation wavelengths. As highlighted in the introduction, time-resolved photoelectron spectroscopy studies of 5-HI have been previously reported using a pump at 273 nm and 249 nm.[22] The absorption onset of the first excited band of 5,6-DHI begins to appear at approximately 315 nm and may be attributed the $S_1(\pi\pi^*)$ state.[17-19] Another excitation band begins to appear strongly at 285-290 nm and is assigned as the second optically bright singlet $\pi\pi^*$state. The predicted energy ordering of this state within the overall singlet manifold varies with the

choice of computational approach,[17-19] but we will adopt the most common assignment of $S_4(\pi\pi^*)$ throughout this communication. The 5,6-DHI absorption features seen in both water and methanol appear red-shifted by as much as 30 nm with respect to the gas phase.[8, 11]

B. TRIY Data

Time-resolved photoion-yield data was recorded for 5,6-DHI using UV pump wavelengths spanning the 241-296 nm region in conjunction with an intense 800 nm multiphoton probe. A representative 3D plot of the transient mass-spectra obtained following 250 nm pump excitation is presented in Fig. 3, revealing a prominent parent ion (m/z = 149) and very minimal fragmentation. A similar lack of significant fragmentation was seen for all pump wavelengths investigated, suggesting that photoionization is achieved via the same photon-order process in all measurements. If higher photon-order ionization became necessary as the pump photon energy was decreased (i.e. a pump + n × probe process no longer exceeded the ionization potential and a pump + (n + 1) × probe process was instead required), the intensity of the fragment ions relative to the parent would be expected to show an associated increase. This is because the total excess energy deposited into the cation would now become greater following ionization. Since this is not seen over the range of pump wavelengths sampled (241-296 nm), we conclude that the 5,6-DHI parent ion was produced predominantly via a 1 + 2′ process in all cases. This consequently puts an upper limit on the ionization potential equal to the energetic equivalent of one 296 nm (4.19 eV) photon (the longest pump wavelength investigated) and two 800 nm photons (2 × 1.55 eV), which is 7.29 eV in total. This observation appears consistent with the theoretical predictions of Mandal *et al.*, who quote vertical and adiabatic ionization potential values of 7.31 eV and 7.00 eV, respectively.[36] We highlight here that two photon ionization at 800 nm potentially leads to quite a restricted view

along the photochemical reaction coordinate and the implications of this are expanded upon in Section IV C.

Focusing in on a reduced *m/z* range (bottom panel of Fig. 3), a large number of very low intensity fragments become visible. The fragment ion transients display a rich array of dynamical behavior, including ultrafast (i.e. sub-picosecond) decay, longer-lived signals and even a strongly rising feature at *m/z* = 120. The various trends seen for each fragment mass are broadly consistent at all pump wavelengths studied. An additional Gaussian feature seen at *m/z* = 32 is a minor contaminant arising due to non-resonant ionization of trace amounts of methanol (utilized when depositing the 5,6-DHI sample onto the thin stainless steel foil). It provides a useful signal, however, serving as an *in situ* reference for the time-zero (i.e. $\Delta t = 0$) position during data acquisition that assists our fitting analysis. In order to ensure that the presence of trace quantities of methanol did not lead to any complex formation that could modify the observed dynamics, test experiments were also performed where 5,6-DHI was deposited onto a foil substrate by simple rubbing (i.e. a solvent-free preparation). Although this less uniform coating produced more overall fluctuation in signal levels, no significant differences in transient behaviour were observed. A summary of the major fragments observed in our experiments and some tentative assignments (aided, in part, by the deuterated measurements recorded at 260 nm) are presented in Table I. No signals were observed in our data at *m/z* values exceeding that of the parent monomer (*m/z* = 149).

It is tempting to try and extract additional information relating to the dynamics operating in the neutral excited states of 5,6-DHI using the fragment transients. This could include weak signatures of higher-order (e.g.1 + 3′) multiphoton ionization producing internally excited cations (which then readily fragment). Higher order photoionization projects more deeply into the

ionization continuum and potentially reveals a more extended view along the reaction coordinate for non-adiabatic relaxation. Alternatively, multiphoton ionization of neutral photofragments formed following dissociation of the parent species could also give rise to some of the observed transients. Both of these processes would potentially provide useful additional insights. Temporal evolution of the fragment ions may, however, also reflect independent dynamical processes operating solely in the parent cation – for example in a 2 + 1′ ionization/excitation process. In this instance, ionization is achieved solely through two-photon absorption of the pump and energy redistribution within the resulting cation may evolve on a different timescale to that of the neutral species. Absorption of an 800 nm photon then probes the cation dynamics by inducing additional prompt fragmentation. When working solely within the one-dimensional measurement framework of a TRIY experiment, it is impossible to decouple the various (independent) neutral and cation dynamical processes that may be contributing to the overall fragment transients. Only further analysis of the parent ions will therefore be considered in detail.

Satisfactory fitting to the TRIY parent ion data using the model described by Eq. 1-2 required one, two or three exponentially decaying functions, depending upon the specific excitation wavelength employed. We label these functions using their respective time constants τ_1 (for ultrafast sub-picosecond dynamics), τ_2 (for signals exhibiting 1/*e* decay constants spanning tens to hundreds of picoseconds) and τ_3 (for very long-lived signals with lifetimes >1 ns). Fig. 4 presents representative fits at pump wavelengths of 292 nm and 250 nm. A summary of the time constants obtained at all pump wavelengths considered is given in Table II, along with the relative fit amplitudes. Although the τ_3 contribution was small, its inclusion was necessary to produce a good

overall fit. Time constant information is also presented graphically in Fig. 5. This clearly illustrates a variation in excited state lifetime with pump energy that is something other than monotonic.

IV. DISCUSSION

A. τ_1 Assignment

At pump wavelengths ≤282 nm, a sub-picosecond lifetime τ_1 is seen in the parent ion transient data (see Table II). One possible origin of this signal is ultrafast intramolecular vibrational energy redistribution (IVR) within the $S_1(\pi\pi^*)$ state. This could lead to a modified Franck-Condon overlap with the cation and an associated change in ionization signal. Such an interpretation is not, however, supported upon comparing the wavelength onset threshold for the appearance of τ_1 with the position of the $S_1(\pi\pi^*)$ state origin (approx. 315 nm, see Fig. 2). This would suggest the onset threshold for IVR is at least 0.45 eV (~3750 cm^{-1}) of internal vibrational energy, which would seem too large for a molecule of low symmetry such as 5,6-DHI (where vibrational coupling restrictions are minimal). Examples reinforcing this point include the IVR onset thresholds previously reported in the $S_1(\pi\pi^*)$ state of anisole (940 cm^{-1}) and hydroquinone (1650 cm^{-1}).[37, 38]

An alternative possibility is that τ_1 describes a decay following excitation of the second optically bright singlet $\pi\pi^*$ state, $S_4(\pi\pi^*)$. This interpretation aligns well with the 5,6-DHI UV absorption spectrum in Fig. 2, where the onset of a second band is seen at approximately 285-290 nm. Quantum chemistry calculations also support this idea, typically predicting the energy separation gap between $S_4(\pi\pi^*)$ and $S_1(\pi\pi^*)$ to be in the 0.4-0.6 eV range.[17-19] This also fits with the relative spectral band positions seen in UV absorption data. Moreover, it has also been predicted that a barrierless conical intersection exists between the $S_4(\pi\pi^*)$and $S_1(\pi\pi^*)$ states.[18] Given this evidence, we therefore attribute τ_1 to ultrafast decay of the $S_4(\pi\pi^*)$ state to $S_1(\pi\pi^*)$. We

note, however, that the range of lifetimes observed (990 fs at 282 nm, falling to 20 fs at 241 nm) suggests that this process may not be completely barrierless. The τ_1 lifetimes may also reflect the extremely rapid decay of other optically bright states sitting energetically above $S_4(\pi\pi^*)$ – particularly at pump wavelengths <270 nm.

B. τ_2 Assignment

Based on the assignment given above, it is logical to now assign the τ_2 lifetime to decay of the $S_1(\pi\pi^*)$ state, which may be populated either directly and/or via internal conversion from $S_4(\pi\pi^*)$ and/or other higher-lying states. Given this assignment it is then interesting to note that the τ_2 lifetimes seen in 5,6-DHI are considerably shorter than those reported at similar pump wavelengths for the decay of the lowest lying $^1\pi\pi^*$ state in 5-HI.[22] Following excitation at 273 nm and 249 nm, these lifetimes in 5,6-DHI are 15 ps and 36 ps, respectively, but in 5-HI no appreciable signal decay was seen at either pump wavelength over the 50 ps pump-probe delay range that was sampled. As highlighted in the Introduction, comparative studies of 5-HI with indole and 4-HI have previously suggested that motion along the O-H bond in 5-HI is not critical for mediating the non-adiabatic dynamics.[21, 22] The apparent differences between 5-HI and 5,6-DHI now lead us to conclude that the proximity of the two OH groups on neighboring carbon atoms exerts a significant effect, and motion along the O5-H coordinate of 5,6-DHI therefore plays a key dynamical role.

Following excitation at 266 nm, $S_1(\pi\pi^*)$ lifetimes of 140 - 180 ps have been reported for 5,6-DHI in aqueous solutions using transient absorption spectroscopy.[8] This is after solvent-mediated relaxation/cooling to the $S_1(\pi\pi^*)$ energy minimum in 5-10 ps. It is interesting to note here that the τ_2 lifetime of 132 ps we observe for the $S_1(\pi\pi^*)$ lifetime in the gas-phase at the longest wavelength pump investigated (296 nm) is similar to these values.

On inspection of Fig. 5, it is clear that the excited state lifetimes display a non-monotonic behaviour with respect to the energy of the pump photon. Within the limits of our experimental error bars, the overall trend in Fig. 5 may initially be viewed as either (i) an exponential decrease in lifetimes with increasing pump energy or (ii) two distinct regions of linear behaviour exhibiting different gradients, with a changeover point between 4.5-4.6 eV (~275-270 nm). The former viewpoint may suggest some sort of tunnelling behaviour is mediating the $S_1(\pi\pi^*)$ state lifetime, whereas the latter is perhaps more indicative of a new pathway for energy dissipation becoming energetically accessible. Our measurements using samples of 5,6-DHI deuterated at the O-H and N-H positions are instructive here: As seen in Table II, deuteration increases both the τ_1 and τ_2 lifetimes by a factor of 1.6-1.7 following 260 nm excitation (200 fs to 320 fs and 22 ps to 37 ps, respectively). The size of this increase is typical for a kinetic isotope effect originating predominantly from zero-point energy effects, rather than from H-atom tunneling, where lifetime increases of 10-100 would reasonably be expected upon deuteration. For example, the gas-phase $S_1(\pi\pi^*)$ lifetime of 4-tert-butylcatechol following 267 nm excitation increases by a factor of 19 upon O-H deuteration as decay of this state proceeds via tunneling under a barrier formed by a $S_1(\pi\pi^*)$/ $S_2(\pi\sigma^*)$ conical intersection.[29]

As detailed in the Introduction, theoretical work by several groups has predicted a conical intersection between the $S_1(\pi\pi^*)$ and $S_2(\pi\sigma^*)$ states of 5,6-DHI. In the longer wavelength (>275 nm) excitation region, τ_2 may therefore reasonably be attributed to this decay pathway. Given the location of the $S_1(\pi\pi^*)$ origin (315 nm), these calculations also indicate that, over the range of excitation energies investigated, the $S_2(\pi\sigma^*)$ state can be populated with sufficient energy to overcome the small (0.3 eV) barrier along O5-H stretch.[18, 19] The implication here is that, once

populated, the (dissociative) $S_2(\pi\sigma^*)$ state will consequently exhibit a very short lifetime, relative to that of $S_1(\pi\pi^*)$. This will lead to steady-state behavior giving rise to an extremely weak $S_2(\pi\sigma^*)$ transient that will be temporally indistinguishable from the decay of the $S_1(\pi\pi^*)$ state.[39] As such, no direct evidence of $S_2(\pi\sigma^*)$ population would be seen in our experimental data.

Based on the predictions of Datar and Hazara,[18] there appear to be two possibilities for the origin of a new energy dissipation pathway in the shorter wavelength excitation region (<275 nm). One of these is the situation where the $S_1(\pi\pi^*)$ internal energy now exceeds the larger (0.63 eV) barrier along the N-H stretching coordinate in the $S_2(\pi\sigma^*)$ state. The other is the onset of a direct route from $S_1(\pi\pi^*)$ to the S_0 ground state, which has a barrier of 0.46 eV with respect to the Franck-Condon minimum. Although our TRIY measurements lack differential sensitivity and so do not provide any conclusive evidence for one alternative over the other, we speculate that the direct S_0 pathway is most likely. The opening up of a second ultrafast decay route within the $S_2(\pi\sigma^*)$ state (presumably working in tandem with O5-H dissociation pathway) would be expected to yield a steeper lifetime vs excitation energy gradient, rather than the shallower trend that is observed (see Fig. 5). On the other hand, direct decay to S_0 may circumvent the $S_2(\pi\sigma^*)$ state and so, although speeding up $S_1(\pi\pi^*)$ decay overall, could give rise to a lifetime vs excitation energy gradient that is independent of that seen for the $S_2(\pi\sigma^*)$ internal conversion pathway.

C. τ_3 Lifetime

Although only exhibiting a weak transient signal, there is a clear long-lived feature seen in TRIY data recorded at excitation wavelengths ≤278 nm (see lower panel of Fig. 4). Over the range of pump-probe delays sampled (up to 200 ps), no apparent decay of this signal was observed and so we quote only a lower bound of $\tau_3 > 1$ ns for the lifetime. At pump wavelengths ≥282 nm, the

τ_3 function was not included in the overall fit due to significant signals associated with τ_2 extending well beyond the pump-probe delay window (see upper panel of Fig. 4). A lifetime component in excess of 1 ns might still reasonably be assumed, however, in this instance. There are two reasonable possibilities for the physical origin of τ_3. One is population of energetically low-lying triplet states via intersystem crossing, as suggested previously in indole,[40] and the other is repopulation of the S_0 ground state.[18, 19] In both cases (and in particular for the S_0 pathway), highly unfavorable Franck-Condon effects make it extremely unlikely that two 800 nm photons will project sufficiently deeply into the continuum to effect efficient ionization. In the case of triplet states, however, the low (<7.3 eV) ionization potential of 5,6-DHI means that three-photon ionization may be sufficient for detection. Relative to two-photon ionization signals that give rise to τ_1 and τ_2, this would yield a weak, but still observable τ_3 signal – as is observed (see Table II). As such, this is our preferred interpretation, although this assignment is tentative and the role of intersystem crossings in 5,6-DHI have not yet been considered theoretically. In Table II it is interesting to note that the relative fit amplitude of the τ_3 component remains largely invariant at all pump wavelengths where it is observed (278-241 nm). This suggests that the fraction of population decaying from $S_1(\pi\pi^*)$ via intersystem crossing is relatively constant over this region, implying this process occurs on a very similar rate to (competing) internal conversion.

V. SUMMARY & OUTLOOK

We have presented the first gas-phase study of the excited state dynamics operating in the key eumelainin sub-unit 5,6-DHI following UV absorption. Sample volatilization was achieved via a laser-based thermal desorption source and permitted a series of time-resolved ion-yield (TRIY) measurements to be undertaken at pump wavelengths spanning the 241 nm - 296 nm

region. Sub-picosecond relaxation of the $S_4(\pi\pi)^*$ state to $S_1(\pi\pi^*)$ was observed following excitation at wavelengths <282 nm. The $S_1(\pi\pi^*)$ state then underwent decay on a timescale that varied between 10 ps and 132 ps as the pump energy decreased. Interestingly, the rate of change in the $S_1(\pi\pi^*)$ lifetime did not display a uniformly monotonic trend with pump energy, and instead exhibited two distinct regions of different gradient. The transition point between these two regions was at 4.5-4.6 eV (~275-270 nm). At lower pump energies, the decay of the $S_1(\pi\pi^*)$ state is attributed to internal conversion to the $S_2(\pi\sigma^*)$ state. At higher pump energy, a new pathway for energy dissipation appears to become energetically accessible, with the most likely candidate being the decay of $S_1(\pi\pi^*)$ direct to the S_0 ground state, as suggested by recent quantum chemistry calculations. The observation of long-lived (>1 ns) features also suggests that triplet state population via intersystem crossing may provide a competing relaxation route. Clear differences also exist between the temporal evolution seen in 5,6-DHI and the related 5-HI system (where N-H motion plays a key role in driving non-adiabatic transitions). The proximity of the two OH groups on neighboring carbon atoms is therefore significant in 5,6-DHI, and motion along the O5-H coordinate now provides a more efficient route for excess energy dissipation and relaxation. This provides a clear illustration of the subtle interplay between molecular structure, dynamics and photochemical function.

Overall, our present findings reveal a great deal of new information about the 5,6-DHI system following UV excitation. There are, however, key questions that remain unanswered – in particular, the relative importance of the different $S_1(\pi\pi^*)$ deactivation pathways in providing any potential photo-protective function. Definitively resolving such issues is beyond the capabilities of the TRIY approach and there is a clear need to conduct new investigations using more differential gas-phase techniques such as time-resolved photoelectron spectroscopy/imaging and

H-atom kinetic energy release measurements. Importantly, however, our initial investigation will permit much more targeted experiments to be performed in future. In particular, comparative studies conducted at pump wavelengths either side of the 275-270 nm region would be particularly instructive in learning more about details of the $S_1(\pi\pi^*)$ relaxation pathways. Furthermore, experiments exciting very close to the $S_1(\pi\pi^*)$ origin (315-300 nm) would potentially also reveal more about the barrier to H-bond extension in the $S_2(\pi\sigma^*)$ state – particularly if the crossover into a tunneling decay regime can be demonstrated. Finally, the role of triplet states remains the subject of some conjecture and more expansive computational chemistry studies are clearly desirable. We therefore hope and anticipate that our initial investigations will serve as a stimulus for new experimental and theoretical undertakings in the near future.

ACKNOWLEDGEMENTS

This work was supported by Leverhulme Trust Research Project Grant RPG-2012-735, and Carnegie Trust Research Incentive Grant 70264 and Engineering and Physical Sciences Council (EPSRC) grant EP/G041717/1. Heriot-Watt University are acknowledged for providing S.W.C. and J.O.F.T. with PhD funding support. We also thank M. J. Paterson for helpful discussions and the National Mass Spectrometry Facility, University of Swansea, for high resolution mass spectra.

REFERENCES

1. J. B. Nofsinger, T. Ye and J. D. Simon, *J. Phys. Chem. B*, 2001, **105**, 2864.
2. Y. Liu and J. D. Simon, *Pigment Cell Res.*, 2003, **16**, 606.
3. T. Ye and J. D. Simon, *J. Phys. Chem. B*, 2003, **107**, 11240.
4. S. P. Nighswander-Rempel, I. B. Mahadevan, H. Rubinsztein-Dunlop and P. Meredith, *Photochem. Photobiol.*, 2007, **83**, 1449.
5. I. R. Piletic, T. E. Matthews and W. S. Warren, *J. Phys. Chem. A*, 2010, **114**, 11483.

6. F. Solano, *Polym. Int.*, 2016, **65**, 1276.

7. B. Marchetti and T. N. V. Karsili, *Phys. Chem. Chem. Phys.*, 2016, **18**, 3644.

8. M. Gauden, A. Pezzella, L. Panzella, A. Napolitano, M. d'Ischia and V. Sundström, *J. Phys. Chem. B*, 2009, **113**, 12575.

9. A. Huijser, A. Pezzella and V. Sundström, *Phys. Chem. Chem. Phys.*, 2011, **13**, 9119.

10. A. Corani, A. Huijser, A. Iadonisi, A. Pezzella, V. Sundström and M. d'Ischia, *J. Phys. Chem. B* 2012, **116**, 13151.

11. J. J. Nogueira, A. Corani, A. El Nahhas, A. Pezzella, M. d'Ischia, L. González and V. Sundström, *J. Phys. Chem. Lett.*, 2017, **8**, 1004.

12. S. Olsen, J. Riesz, I. Mahadevan, A. Coutts, J. P. Bothma, B. J. Powell, R. H. McKenzie, S. C. Smith and P. Meredith, *J. Am. Chem. Soc.*, 2007, **129**, 6672.

13. A. Huijser, A. Pezzella, J. K. Hannestad, L. Panzella, A. Napolitano, M. d'Ischia and V. Sundström, *ChemPhysChem*, 2010, **11**, 2424.

14. A. Corani, A. Pezzella, T. Pascher, T. Gustavsson, D. Markovitsi, A. Huijser, M. d'Ischia and V. Sundström, *J. Phys. Chem. Lett.*, 2013, **4**, 1383.

15. A. Corani, A. Huijser, T. Gustavsson, D. Markovitsi, P.-Å. Malmqvist, A. Pezzella, M. d'Ischia and V. Sundström, *J. Am. Chem. Soc.*, 2014, **136**, 11626.

16. O. Ghafur, S. W. Crane, M. Ryszka, J. Bockova, A. Rebelo, L. Saalbach, S. De Camillis, J. B. Greenwood, S. Eden and D. Townsend, *J. Chem. Phys.*, 2018, **149**, 034301.

17. A. L. Sobolewski and W. Domcke, *ChemPhysChem*, 2007, **8**, 756.

18. A. Datar and A. Hazra, *J. Phys. Chem. A*, 2017, **121**, 2790.

19. P. Ghosh and D. Ghosh, *J. Phys. Chem. B*, 2017, **121**, 5988.

20. S. Matsika and P. Krause, *Annu. Rev. Phys. Chem.*, 2011, **62**, 621.

21. T. A. A. Oliver, G. A. King and M. N. R. Ashfold, *Phys. Chem. Chem. Phys.*, 2011, **13**, 14646.

22. R. Livingstone, O. Schalk, A. E. Boguslavskiy, G. Wu, L. T. Bergendahl, A. Stolow, M. J. Paterson and D. Townsend, *J. Chem. Phys.*, 2011, **135**, 194307.

23. Y. Huang and M. Sulkes, *Chem. Phys. Lett.*, 1996, **254**, 242.

24. S. Arnold, L. Tong and M. Sulkes, *J. Phys. Chem.*, 1994, **98**, 2325.

25. M. Sulkes and I. Borthwick, *Chem. Phys. Lett.*, 1997, **279**, 315.

26. R. A. Livingstone, J. O. F. Thompson, M. Iljina, R. J. Donaldson, B. J. Sussman, M. J. Paterson and D. Townsend, *J. Chem. Phys.*, 2012, **137**, 184304.

27. A. S. Chatterley, J. D. Young, D. Townsend, J. M. Żurek, M. J. Paterson, G. M. Roberts and V. G. Stavros, *Phys. Chem. Chem. Phys.*, 2013, **15**, 6879.

28. G. M. Roberts, A. S. Chatterley, J. D. Young and V. G. Stavros, *J. Phys. Chem. Lett.*, 2012, **3**, 348.

29. M. D. Horbury, L. A. Baker, W.-D. Quan, J. D. Young, M. Staniforth, S. E. Greenough and V. G. Stavros, *J. Phys. Chem. A*, 2015, **119**, 11989.

30. S. P. H. Mee, V. Lee, J. E. Baldwin and A. Cowley, *Tetrahedron*, 2004, **60**, 3695.

31. J. D. Benigni and R. L. Minnis, *J. Heterocycl. Chem.*, 1965, **2**, 387.

32. United States Environmental Protection Agency, https://comptox.epa.gov, (accessed November 2018).

33. F. Calegari, A. Trabattoni, A. Palacios, D. Ayuso, M. C. Castrovilli, J. B. Greenwood, P. Decleva, F. Martín and M. Nisoli, *J. Phys. B: At. Mol. OPt. Phys.*, 2016, **49**, 142001.

34. C. R. Calvert, L. Belshaw, M. J. Duffy, O. Kelly, R. B. King, A. G. Smyth, T. J. Kelly, J. T. Costello, D. J. Timson, W. A. Bryan, T. Kierspel, P. Rice, I. C. E. Turcu, C. M. Cacho, E. Springate, I. D. Williams and J. B. Greenwood, *Phys. Chem. Chem. Phys.*, 2012, **14**, 6289.

35. Y. V. Il'ichev and J. D. Simon, *J. Phys. Chem. B*, 2003, **107**, 7162.

36. M. Mandal, T. Das, B. K. Grewal and D. Ghosh, *J. Phys. Chem. B*, 2015, **119**, 13288.

37. R. Matsumoto, K. Sakeda, Y. Matsushita, T. Suzuki and T. Ichimura, *J. Mol. Struct.*, 2005, **735**, 153.

38. G. N. Patwari, S. Doraiswamy and S. Wategaonkar, *J. Phys. Chem. A*, 2000, **104**, 8466.

39. N. Kotsina and D. Townsend, *Phys. Chem. Chem. Phys.*, 2017, **19**, 29409.

40. S.-T. Park, A. Gahlmann, Y. He, J. S. Feenstra and A. H. Zewail, *Angew. Chem. Int. Ed.*, 2008, **47**, 9496.

Table Captions

Table I: Summary and some tentative assignments of the various major fragment ions produced from 5,6-DHI following UV excitation over the 241 - 296 nm region and subsequent ionization with an intense 800 nm probe.

Table II: 1/*e* decay lifetimes τ_i and relative fit amplitudes a_i for 5,6-DHI over the 241 - 296 nm excitation region, obtained using the sequential fitting procedure described by Eq. (1) and (2). Quoted uncertainties are 1σ values. At wavelengths ≥282 nm τ_3 lifetimes are labelled as n/a since a long-lived function was not included in the overall fit (due to significant signals associated with τ_2 extending far beyond the experimental pump-probe delay window). A lifetime component > 1 ns may still reasonably be assumed, however, given the excitation data at pump wavelengths <282 nm.

Table I

m/z	Fragment assignment
1	H^+
15	CH_3^+
28	CO^+ and CH_2N^+
32	CH_4O^+ (methanol contaminant)
39/40	?
42/43	?
51/52	?
65/66	?
75	$C_6H_3^+$ and/or C_5HN^+
92/93	?
103	$C_7H_5N^+$
120	$C_7H_6NO^+$ (loss of COH)
132	$C_8H_6NO^+$ (loss of OH)

Table II

λ_{pump} (nm)	Energy (eV)	τ_1 (fs)	τ_2 (ps)	τ_3	$a_1 : a_2 : a_3$
241	5.14	20 ± 10	10 ± 5	>1 ns	1.85 : 1.00 : 0.04
250	4.96	100 ± 30	15 ± 5	>1 ns	0.85 : 1.00 : 0.03
260	4.77	200 ± 50	22 ± 5	>1 ns	0.64 : 1.00 : 0.02
*260**	*4.77*	*320 ±50*	*37 ±5*	*>1 ns*	*0.82: 1.00: 0.02*
267	4.64	275 ± 100	30 ± 5	>1 ns	0.85 : 1.00 : 0.01
273	4.54	325 ± 100	36 ± 5	>1 ns	0.83 : 1.00 : 0.02
278	4.46	600 ± 150	51 ± 5	>1 ns	0.87 : 1.00 : 0.03
282	4.40	990 ± 150	73 ± 5	n/a	1.01 : 1.00 : -
287	4.32	-	95 ± 5	n/a	- : 1.00 : -
292	4.25	-	122 ± 5	n/a	- : 1.00 : -
296	4.19	-	132 ± 5	n/a	- : 1.00 : -

* 5,6-DHI deuterated at OH and NH positions

Figure Captions

Figure 1: Schematic structures of indole, the eumelanin building blocks 5,6-dihydroxyindole and 5,6-dihydroxyindole-2-carboxylic acid, and the monohydroxyindoles 4-, 5- and 6-hydroxyindole. For indole, the 4, 5 and 6 carbon atom positions are indicated, and these labels also apply for the other species presented. In the various hydroxyindoles, the oxygen atoms are denoted using the same number label as the carbon atom to which they are attached (e.g. O5-H etc.).

Figure 2: UV absorption spectra of 5,6-dihydroxyindole, the monohydroxyindoles 4-, 5- and 6-hydroxyindole, as well as the bare indole chromophore (0.2 nm scan interval/1 mm slit width). Samples were dissolved in cyclohexane providing spectra analogous to the gas phase.

Figure 3: (Top) TRIY plot obtained for 5,6-DHI utilizing a 250 nm pump and an intense 800 nm probe. (Bottom) ×20 zoomed in view of the 5,6-DHI fragment ions, which exhibit a range of different transitory behaviors. The time axes are linear up to 1 ps and logarithmic beyond this point.

Figure 4: Representative parent ion transients and associated fits for 5,6-DHI presented on a mixed linear-logarithmic timescale. Also shown are the associated residuals (i.e. the overall fit minus the raw data). Top: 292/800 nm pump/probe. Bottom: 250/800 nm pump/probe. Errors quoted in numerical time constants are 1σ values.

Figure 5: Plots of the τ_1 (top) and τ_2 (bottom) 1/*e* lifetimes extracted from fits to the 5,6-DHI parent ion transients obtained at a range of pump energies. The overall fitting model is described in Eq. 1-2. Error bars denote 1σ uncertainties.

Figure 1

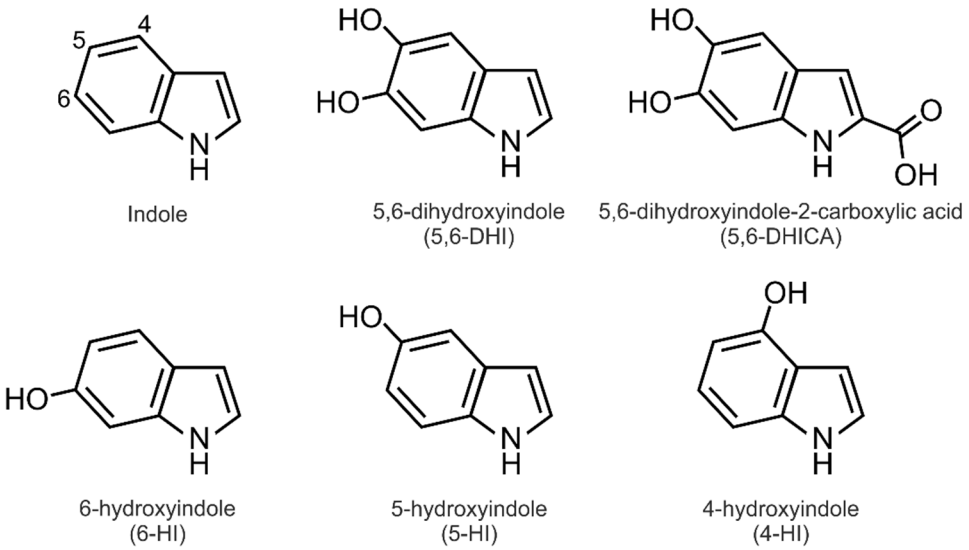
5
4
6
N
H
Indole
HO
HO
N
H
5,6-dihydroxyindole
(5,6-DHI)
HO
HO
N
H
O
OH
5,6-dihydroxyindole-2-carboxylic acid
(5,6-DHICA)
HO
N
H
6-hydroxyindole
(6-HI)
HO
N
H
5-hydroxyindole
(5-HI)
OH
N
H
4-hydroxyindole
(4-HI)

Figure 2

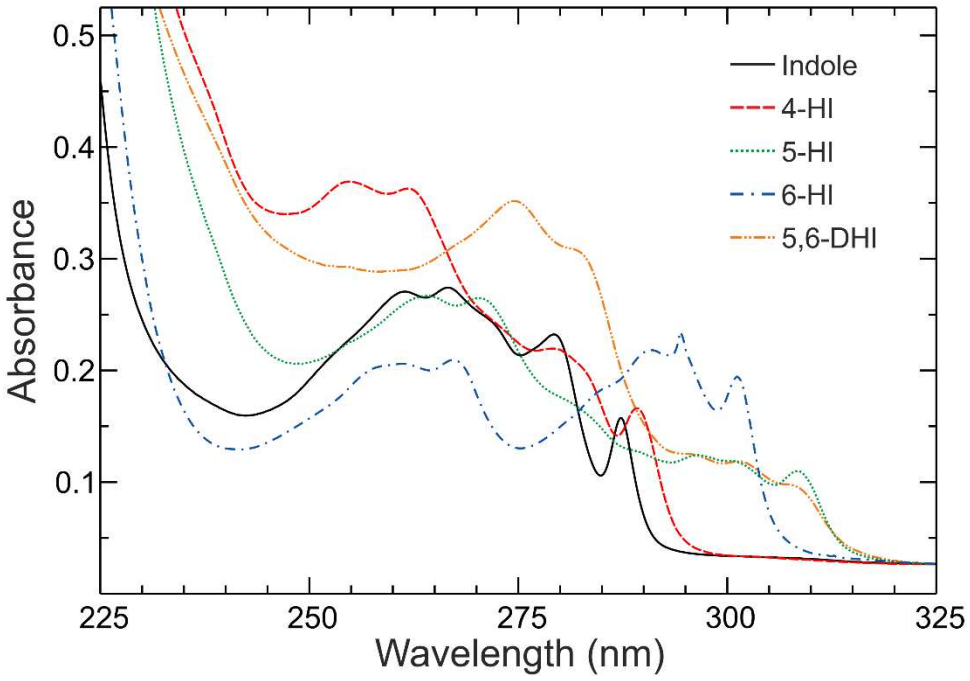
Absorbance
Wavelength (nm)
0.5
0.4
0.3
0.2
0.1
225
250
275
300
325
Indole
4-HI
5-HI
6-HI
5,6-DHI

Figure 3

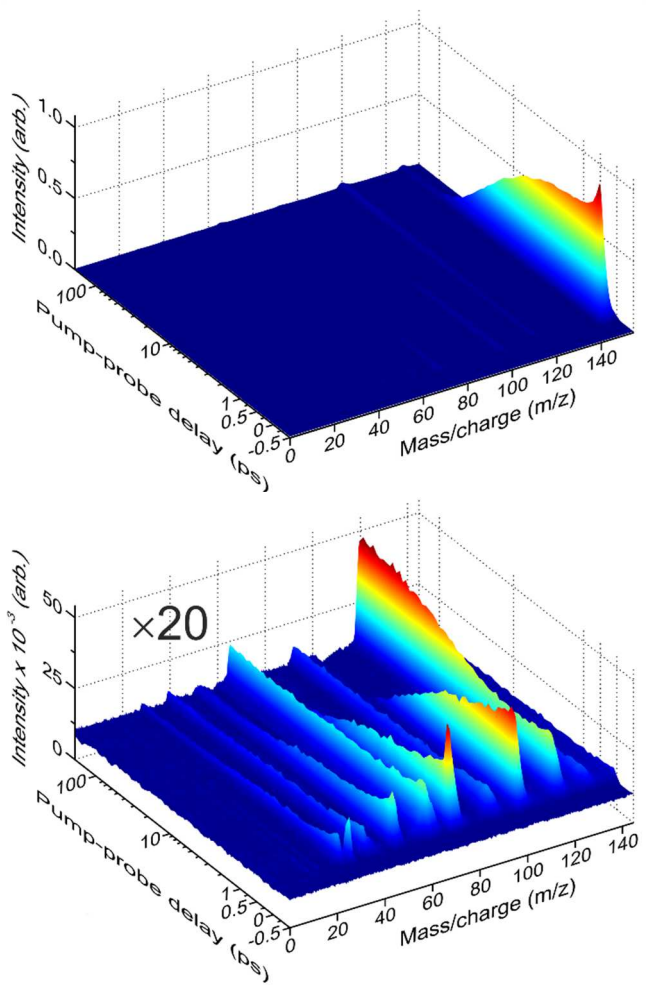
Intensity (arb.)
1.0
0.5
0.0
100
10
1
0.5
0
-0.5
Pump-probe delay (ps)
0
20
40
60
80
100
120
140
Mass/charge (m/z)
Intensity x 10^-3 (arb.)
50
25
0
×20
100
10
1
0.5
0
-0.5
Pump-probe delay (ps)
0
20
40
60
80
100
120
140
Mass/charge (m/z)

Figure 4

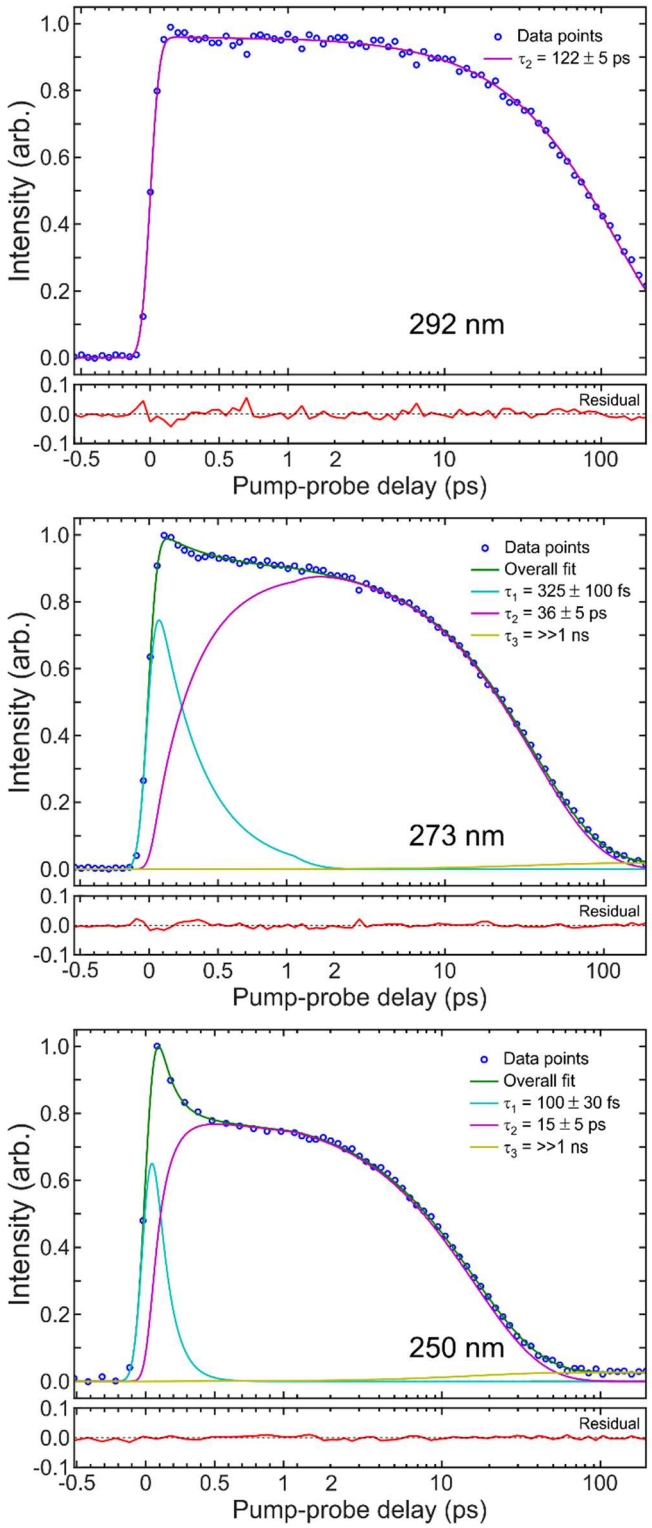
Data points
τ2 = 122 ± 5 ps
292 nm
Residual
Intensity (arb.)
Pump-probe delay (ps)
Data points
Overall fit
τ1 = 325 ± 100 fs
τ2 = 36 ± 5 ps
τ3 = >>1 ns
273 nm
Residual
Intensity (arb.)
Pump-probe delay (ps)
Data points
Overall fit
τ1 = 100 ± 30 fs
τ2 = 15 ± 5 ps
τ3 = >>1 ns
250 nm
Residual
Intensity (arb.)
Pump-probe delay (ps)

Figure 5

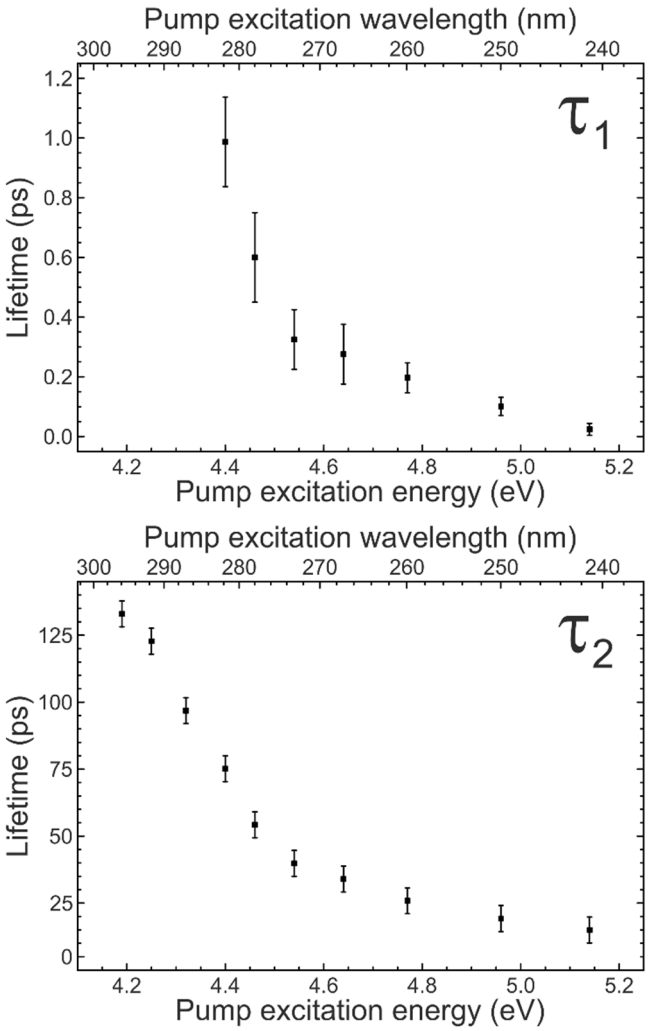
Pump excitation wavelength (nm)
300 290 280 270 260 250 240
1.2
1.0
0.8
0.6
0.4
0.2
0.0
Lifetime (ps)
τ1
4.2 4.4 4.6 4.8 5.0 5.2
Pump excitation energy (eV)
Pump excitation wavelength (nm)
300 290 280 270 260 250 240
125
100
75
50
25
0
Lifetime (ps)
τ2
4.2 4.4 4.6 4.8 5.0 5.2
Pump excitation energy (eV)